

# IMPROVEMENT OF SHIP DETECTION ACCURACY BY SAR MULTI-LOOK CROSS-CORRELATION TECHNIQUE USING ADAPTIVE CFAR

Kazuo Ouchi , *Senior Member, IEEE* and Seong-In Hwang, *Non-Member, IEEE*

Department of Information Science, School of Electrical and Computer Engineering  
National Defense Academy, 1-10-20, Hashirimizu, Yokosuka 239-8686, Japan.

## 1. INTRODUCTION

In recent years, there is a growing interest in ship detection, classification and identification by synthetic aperture radar (SAR) for its ability of all-weather and day-and-night operational capability. The reasons behind this trend are increasing marine crimes such as sea piracy, identification of ships responsible for oil pollution, and illegally operating ships. Some algorithms and ship detection systems have been proposed and tested, including those based on amplitude threshold, intensity  $K$ -distribution, combination with ship wake detection, wavelet transform, polarimetric analyses, constant false alarm rate (CFAR), and multi-look cross-correlation (MLCC) [1]-[10]. Different algorithms show different performance with certain room for improvements. One of the requirements for future ship detection systems is the accuracy improvement for detecting small ships with lower false alarm rate (FAR) [11]. For this purpose, we carried out an experiment of detecting small fishing boats whose sizes are comparable with the resolution cell of the Phased Array L-band SAR (PALSAR) on board of the Japanese Advanced Land Observing Satellite (ALOS) [10]. Among the algorithms considered in the experiment, we found that the MLCC algorithm could be improved by applying CFAR to the coherence images computed by MLCC. The present paper describes the summary of the ship detection by MLCC-CFAR applied to ALOS-PALSAR data: the detailed result can be referred to our recent publication [12].

## 2. EXPERIMENTAL PROCEDURE

The principle of the MLCC algorithm is first to produce two (or more) independent sub-images of a same scene from SAR raw data using sub-apertures of different center frequencies [4]. This multi-look processing is the basis of speckle reduction, i.e., inter-look random noise patterns are uncorrelated, while the images of deterministic targets are correlated. The procedure is then to compute the degree of cross-correlation between the sub-images using a small moving window. If the window contains only noise from the sea surface, the degree of cross-correlation is low, but if it contains the image of a ship, the degree of inter-look cross-correlation is high. Thus, the images of ships can be extracted by thresholding the coherence image which is a map of the degree of inter-look cross-correlation. The main problem is that it is difficult to automatically find the optimum threshold value for the coherence image. A solution to this problem is to apply CFAR to the inter-look coherence image. This process of the MLCC-CFAR algorithm is illustrated I Fig.1.

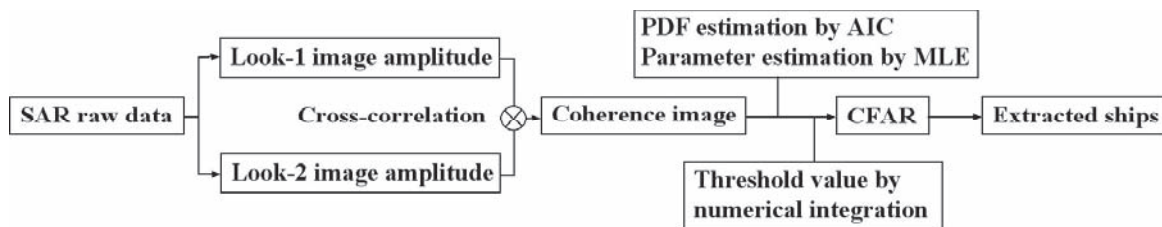


Fig. 1 Block diagram of MLCC-CFAR processing for automatic detection of ships and accuracy improvement.

Boat type	Type Ia, b	Type IIa, b	Type IIIa, b
Length [m]	12.0, 14.6	10.7, 11.9	8.0, 9.2
Width [m]	3.0, 4.0	3.2, 3.2	2.4, 2.5
Depth [m]	1.2, 2.0	1.1, 1.0	0.8, 1.1
Tonnage [tons]	11.2, 12.0	6.6, 9.7	2.2, 3.2



Fig.2 Parameters of the fishing boats used for the experiment (left) and a picture of Type Ib boat (right).

In order to apply CFAR to a MLCC coherence image, a probability density function (PDF) which fits best to the image amplitude inside the moving window is sought. The moving window size was 9 x 9 pixels by taking into account the size of the fishing boats relative to the PALSAR resolution cell. By comparing the Akaike information criterion (AIC) [13] of Gamma, Weibull, Lognormal, and Rayleigh distributions, the Lognormal distribution was found to fit best to almost all data. Having selected the best PDF, the parameters for the estimated PDF were calculated by maximum likelihood estimation (MLE), and the threshold value was computed from numerical integration in an adaptive way for different positions of the moving window. For the computation of the threshold value, a probability false alarm (PFA) was set. Finally, the CFAR algorithm was applied to the inter-look coherence image to extract the fishing boats.

In the experiment, three fishing boats of different sizes were deployed in the Tosa Bay, Kochi Japan as in Fig.2. The Type I boat was positioned approximately 1 km away from the shore, followed by Type II and Type III separated by 50 m. The largest boat Type I started cruising toward the corner reflector placed on the beach (see Fig.3) with the speed of 8 knots (4.12 m/s) at 10 minutes before the PALSAR data acquisition, and with two minutes time interval, Type II and Type III followed. The experiment was made at different PALSAR modes: FBS (Fine Beam Single) 21.5 HH, FBS 34.3 HH, FBD (Fine Beam Double) 41.5 HH/HV, and PLR (PoLaRimetric) 20.5 HH/HV/VH/VV, where the numbers after the modes are the off-nadir angles in degrees. Analyses were carried out for the FBS data only, and FBD and PLR data were not considered because they were not suitable for ship detection due to coarse resolution [10]. The FBS 21.5 and 34.3 data were acquired in June 21 and July 30, both in 2006 and the resolution was 4.1 m in azimuth and 4.7 in range direction for both the data. The wind speed was 2.0 m/s and 1.0 m/s, and significant waveheight was 0.49 m and 0.35 m at the data acquisition times of FBS 21.5 and 34.3 respectively.

### 3. RESULTS AND DISCUSSION

The amplitude image of FBS 34.5 data is shown in Fig.3(a), where the Type Ib, IIa, and IIIa boats are all visible. By applying AIC to the amplitude images, the Weibull distribution was found to fit best to the data, followed by *K*-distribution, Rayleigh, Gamma and Lognormal distributions [10]. The coherence image computed from the 2-look images is shown in Fig.3(b) where the degrees of interlook coherence are also high for all three boats. From the AIC result, the coherence image was found to fit best to the Gamma distribution, followed by Lognormal, Weibull, and Rayleigh distributions. It should be noted that the transition of Weibull-distributed amplitude fluctuations to Gamma-distributed fluctuations in the coherence image was found by simulation and from the real data. Its theoretical interpretation requires further study. Fig.3(c) is the enlarged image containing three boats. In order to extract the boats, the coherence image is thresholded with the threshold value defined by  $C_T = \langle C \rangle + N \cdot \text{STD}$ , where  $\langle C \rangle$  is the mean coherence value, STD is the standard deviation within the moving window, and *N* is the thresholding parameter. In the thresholding process, pixels of values below  $C_T$  are replaced by zero. Fig.3(d) and (e) are the coherence images after thresholding with *N*=2 and 6 respectively. It can be seen from Fig.3(d) that when *N*=2 all boats are visible but some surrounding noise is also present, and that by increasing the threshold parameter to *N*=6, surrounding noise decreases, but the image of Type IIIa boat also disappears as in Fig.3(e). On the other hand, all boats can be detected by applying MLCC-CFAR with little surrounding noise as in Fig.3(f).

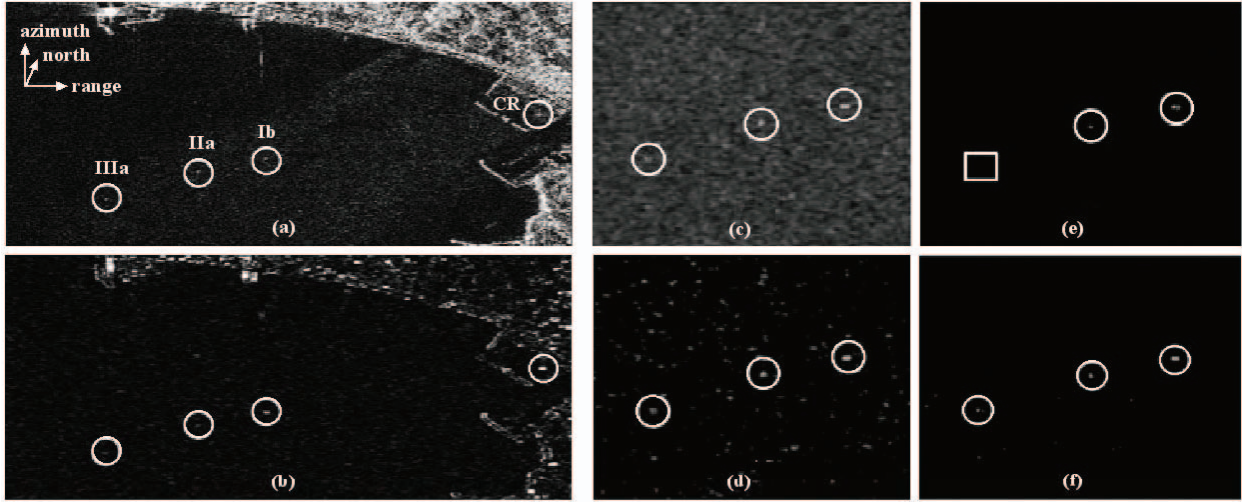


Fig. 3 The images (a) and (b) correspond respectively to the amplitude and coherence image after applying MLCC to the FBS 34.3 data. The image (c) is an enlarged coherence image, and those (d) and (e) show the images after thresholding the coherence image (c) with the threshold parameter  $N=2$  and  $6$  respectively. The white circles indicate the detected boats, and the white square implies an undetected boat. The image (f) is the result after MLCC-CFAR applied to the image (c). The image size of (a) and (b) is approximately 2.1 km in azimuth and 3.8 km in range direction. “CR” on the center-right is a triangular trihedral corner reflector of short-sided size 1.98 m (the theoretical RCS of 30.6 dB) placed on the beach for the purpose of PALSAR calibration.

PALSAR Modes	MLCC ( $N=2$ )	MLCC ( $N=4$ )	MLCC ( $N=6$ )	MLCC-CFAR
FBS 34.3	$2.74 \times 10^{-2}$ (3)	$7.31 \times 10^{-4}$ (3)	$3.56 \times 10^{-4}$ (2)	$2.17 \times 10^{-4}$ (3)
FBS 21.5	$3.06 \times 10^{-2}$ (3)	$9.83 \times 10^{-4}$ (2)	$2.50 \times 10^{-5}$ (0)	$8.88 \times 10^{-3}$ (3)

Table 1. Comparison of FAR by thresholding the coherence images with different threshold parameters  $N$  and the adaptive MLCC-CFAR method. The numbers inside the brackets show the number of detected boats.

PALSAR Modes	Boat Type	$N=0$	$N=2$	$N=4$	$N=6$	MLCC-CFAR
FBS 34.3	Ib	25.6	32.0	59.9	64.7	66.9
	IIa	22.9	29.6	59.5	63.6	65.7
	IIIb	21.6	27.6	51.0	0.0	65.4
FBS 21.5	Ia	15.6	28.6	43.8	0.0	38.3
	IIa	17.4	29.9	44.1	0.0	34.8
	IIIa	15.6	22.8	0.0	0.0	31.6

Table 2. Comparison of signal to background noise ratio [dB] by thresholding the coherence images with different threshold parameters  $N$  and the adaptive MLCC-CFAR method.

The quantitative interpretation of Fig.3 is to compute the FAR values as listed in Table 1. By simple thresholding the coherence image, the FAR values decrease with increasing  $N$ , but the Type IIIb boat cannot be detected when  $N=6$  in the FBS 34.3. While, using MLCC-CFAR all three boats can be detected with a lower FAR value. The same trend can be seen for the FBS 21.5 data. For the FBS 21.5 data, the detection accuracy is lower because of

higher sea state and smaller radar depression angle. As a result, Type IIIa boat disappears when  $N=4$ , and all boats cannot be extracted when  $N=6$ , but again using MLCC-CFAR all boats can be detected as in Table 1.

The magnitude of the coherence image of a boat is defined as the mean signal coherence amplitude divided by the mean background amplitude with zero pixel values below  $C_T$ . This measure is termed as SNR (Signal to Noise Ratio) for convenience. Table 2 shows the SNR for individual boats, where a similar trend as for FAR can be seen. That is, SNR after thresholding of coherence images increases with increasing  $N$ , but drops to zero for the Type IIIa when  $N=6$  for FBS 34.3, and for Type IIIa when  $N=4$  and all boats when  $N=6$  in FBS 21.5. This is because the signal amplitude is also thresholded out when  $N$  becomes large and replaced by zero. Again, MLCC-CFAR shows satisfactory performance in the SNR values for all coherence images of the fishing boats.

#### 4. ACKNOWLEDGEMENT

The raw PALSAR data were provided by Japan Aerospace Exploration Agency (JAXA) and processed at National Defense Academy (NDA) of Japan under the research agreement for the ALOS between JAXA and NDA.

#### REFERENCES

- [ 1 ] K. Eldhuset, "An automatic ship and ship wake detection system for spaceborne SAR images in coastal regions," *IEEE Trans. Geosci. Remote Sens.*, vol.34, pp.1010-1019, 1996.
- [ 2 ] M. F. Fingas and C. E. Brown, "Review of ship detection from airborne platforms," *Canadian J. Remote Sens.*, vol.27, no.4, pp.379-385, 2001.
- [ 3 ] J.M. Kuo and K.S. Chen, "The application of wavelet correlator for ship wake detection," *IEEE Trans. Geosci. Remote Sens.*, vol.41, pp.1506-1511, 2003.
- [ 4 ] D.J. Crisp, *The State-of-the-Art in Ship Detection in Synthetic Aperture Radar Imagery*, Defence Science and Technology Organization (DSTO) Information Science Laboratory, Edinburgh, Australia, 2004. [Online]. Available: <http://www.dsto.defence.gov.au/publications/2660/DSTO-RR-0272.pdf>.
- [ 5 ] K. Ouchi, S. Tamaki, H. Yaguchi, and M. Iehara, "Ship detection based on coherence images derived from cross-correlation of multilook SAR images," *IEEE Trans. Geosci. Remote Sens. Lett.*, vol.1, pp.184-187, 2004.
- [ 6 ] M. Tello, C. Lopez-Martinez, and J.J. Mallorqui, "A novel algorithm for ship detection in SAR imagery based on the wavelet transform," *IEEE Geosci. Remote Sens. Lett.*, vol.2, no., pp.201-205, 2005.
- [ 7 ] H. Greidanus and N. Kourti, "Finding of the DECLIMS project-detection and classification of marine traffic control," *Proc. SEASAR 2006, Frascati, Italy (ESA SP-613)*, 2006.
- [ 8 ] G. Margarit, J.J. Mallorqui, J.M. Rius, and J. Sanz-Marcos, "On the usage of GRECOSAR, an orbital polarimetric SAR simulator of complex targets, to vessel classification studies," *IEEE Trans. Geosci. Remote Sens.*, vol.44, no.12, pp.3517-3526, 2006.
- [ 9 ] G. Margarit, J.J. Mallorqui, J. Fortuny-Guasch, and C. Lopez-Martinez, "Exploitation of ship scattering in polarimetric SAR for an improved classification under high clutter conditions," *IEEE Trans. Geosci. Remote Sens.*, vol.47, no.4, pp.1224-1235, 2009.
- [ 10 ] S-I. Hwang, H. Wang, and K. Ouchi, "Comparison and evaluation of ship detection and identification algorithms using small boats and ALOS-PALSAR," *IEICE Trans. Commun.*, vol.E92-B, no.12, pp.3883-3892, 2009.
- [ 11 ] H. Greidanus, *DECLIMS : Requirements for Future Systems*, Joint Research Center, European Commission DECLIMS homepage. [Online]. Available: <http://declims.jrc.ec.europa.eu>.
- [ 12 ] S-I. Hwang and K. Ouchi, "On a novel approach using MLCC and CFAR for the improvement of ship detection by synthetic aperture radar," *IEEE Geosci. Remote Sens. Lett.*, vol.7, no 2, 2010 (in press).
- [ 13 ] H. Akaike, "Information theory and an extension of the maximum likelihood principle," *Proc. 2nd International Symposium on Information Theory*, pp.267-281, 1973.